Paper:
Nabavi, S., Farshidianfar, A., Afsharfard, A. & Khodaparast, H. (2018). An ocean wave-based piezoelectric energy harvesting system using breaking wave force. *International Journal of Mechanical Sciences*
http://dx.doi.org/10.1016/j.ijmecsci.2018.12.008

An ocean wave-based piezoelectric energy harvesting system using breaking wave force

Seyedeh Fatemeh Nabavi , Anooshiravan Farshidianfar ,
Aref Afsharfard , Hamed Haddad Khodaparast

PII: S0020-7403(18)31966-0
DOI: https://doi.org/10.1016/j.ijmecsci.2018.12.008
Reference: MS 4666

To appear in: *International Journal of Mechanical Sciences*

Received date: 14 June 2018
Revised date: 22 November 2018
Accepted date: 4 December 2018

Highlights:

- The breakwater and vibration-based energy harvesting systems are combined.
- A low-volume piezoelectric energy harvesting system is studied analytically.
- The analytical model is updated using experimental data.
- Four possible conceptual designs for energy harvesting systems are proposed and studied.

An ocean wave-based piezoelectric energy harvesting system using breaking wave force

Seyedeh Fatemeh Nabavi[1], Anooshiravan Farshidianfar[1], Aref Afsharfard[1,*], Hamed Haddad Khodaparast[2]
[1]Mechanical Engineering Department, Ferdowsi University of Mashhad, Mashhad, Iran
[2]College of Engineering, Swansea University, Swansea, UK

Abstract
Nowadays, in the case of the coastal structures, wave breaking and access to clean energy are two important issues, which can be addressed by combining breakwater and vibration-based energy harvesting systems. In this study, the mechanical energy which is produced when ocean wave breaks into a vertical face is converted into electrical energy. To accomplish this, a new low-volume piezoelectric beam-column energy harvesting system is proposed. To study the application of this system, a theoretical model is presented and studied analytically. The analytical model is updated using experimental data and it is shown that the analytical results were similar to the experimental results after updating. After validating the electromechanical model, an energy harvesting system is presented, which can produce energy from breaking ocean waves on a vertical face. Four possible conceptual designs for energy harvesting systems are considered and the so-called Perfection Rate (*PR*) is introduced to select the best model to maximize harvested energy whilst mitigating the deteriorating effects of large strain deformation.
Keywords: Energy harvesting; Breaking waves; Piezoelectric; Modal updating; Experimental study

1- Introduction

As 70% of Earth's surface is ocean [1], wave energy is an attractive source for scientists and engineers [2-9]. The potential electrical energy that can be generated from ocean waves is estimated to be over 885 TWh annually [5]. Regarding this potential, different systems are proposed to convert ocean wave energy into electrical energy. Generally, Wave Energy Converters (WEC) are divided into three major types: (a) offshore, such as oscillating-body wave energy converters, (b) nearshore, such as oscillating water columns and (c) in shore or shoreline such as overtopping devices [10]. Each of the discussed WEC's have advantages and disadvantages. Liang *et al.* proposed a novel offshore system which could convert bidirectional wave motion into unidirectional rotation of generator shafts. To do so, they used two one-way bearings in a rack and pinion system [11, 12]. Because of the distance from the coastline, long power transmission lines are needed in the case of offshore WEC's. The challenges presented by offshore structures is studied by Scruggs and Jacob [13]. Nearshore WEC's simultaneously amplify weakness points and weaken strength points of offshore and shoreline WEC's. In the case of shoreline devices which are placed on the coastline, although the energy density of ocean waves is not high, complicated power transmission lines are not needed. It should be noted that one of the important parts of WEC's is the transducer that converts collected mechanical energy into electrical energy. In 2013, a novel triboelectric Nano-generator was built on a suspended 3D spiral structure [14].

Despite the high-level output, the main problem of WECs is the high construction cost. Thus, economic concerns are one of the crucial issues in the future commercialization of the WEC. Coupling of these systems with existing coastal structures is a possible way to reduce economic issues. Meanwhile, shoreline WECs are appealing because the cost of construction and maintenance is reduced and their utilization is economic [14]. For this reason, different types of hybrid breakwaters including Oscillating Water Columns (OWC) [15-17], rubble

* Corresponding Author: Aref Afsharfard
Email: afsharfard@um.ac.ir

mound overtopping [18-22], and floating breakwater devices [23-26] have recently been studied by many researchers. The combining of breakwater systems with WECs has many benefits. Besides reducing the cost of utilization, construction and operation, these systems do not require additional space and the scenery of the surrounding environmental is not affected.

Among the variety of WECs, multipurpose coastal structures and ocean wave energy convertors have received a lot of attention in the last decades. The WEC method of overtopping breakwater has been the subject of previous studies [18-22]. These systems consist of input force, breakwater, absorber, transducer and other aspects. Several studies have been carried out on WECs which work with floating breakwaters [25, 26]. Boccotti presented a new design breakwater WEC which works based on entrapping ocean flow [27]. Buccino *et al.* analyzed a low-head composite sea wall energy converter device [18]. He *et al.* studied the application of an OWC combined with slack-moored breakwater for a range of frequencies [23]. Peng *et al.* investigated the application of a pontoon-type floating breakwater in an intermediate water depth [24]. The effect of mooring angle and the length of the floating part on output power was investigated. Malara demonstrated the reliability of U-oscillating water columns device [16]. Ning studied the application of a dual-chamber OWC and the effect of wave conditions on its performance [17]. Viet *et al.* studied energy harvesting from intermediate and deep water waves using piezoelectric materials [28].

Many studies in recent years have focused on energy harvesting systems [29-32]. These include the application, theory and design of these systems. Euler Bernoulli theory for piezoelectric beam-columns is one approach which is applicable in this area of research[33]. In addition, decreasing the occupied volume of the energy harvesting system, which is one of main aims of this study, has been considered in previous studies [34].

In floating breakwater devices, the different movements of breakwater (heave, pitch, roll, sway, surge and yaw) distribute the wave forces and lead to undesired damp wave energy. The purpose of this study is to present a novel system which can provide sufficient electrical output from the heave motion of breakwater. Here, because of the high amplitude of breaking wave force, it is used as input force. Note that in reality, breaking waves have a wide frequency band, mainly within low frequency range. Furthermore, wave-based energy harvesting systems should be designed in a way that their natural frequencies lie within the frequency range of the breaking wave. To achieve this, the vibration-based energy harvesting system should generally be large. The proposed energy harvesting system in this paper, not only is small, but also has a fundamental frequency in low frequency range. In other words, another feature of the proposed device is that the system frequency is tunable, which allows the system to synchronize in different frequency ranges.

To study the proposed system, firstly, the electromechanical behavior of the harvesting device is investigated in section 2. The governing electromechanical equation for the system is obtained and validated in this section. The ocean wave-based energy harvesting device is introduced in section 3. Finally, the vibratory application and different configurations of the presented system are analyzed in section 4.

2- Electromechanical behavior of energy harvester

2-1- Analytical approach

The system proposed for energy harvesting is a complex clamped-guided beam-column structure with tip masses M_{tip2} and M_{tip1} as shown in Figure (1-A). Note that unlike large-scale systems which can work with low frequency excitation, to work efficiently small-scale systems should be excited with high frequency. The presented beam-column piezoelectric structure is a novel structure which prepares the small-size system to work with low frequency excitation. The length (L), density (ρ), thickness (t) and flexural stiffness (EI) are considered. Subscribes b and p stand for beam and piezoelectric parts respectively. The clamped-guided piezoelectric structure is connected to a moving mass (M_{base}), which is exposed to produce base excitation from external load F. Figure (1-B) shows the electrical circuit of the system.

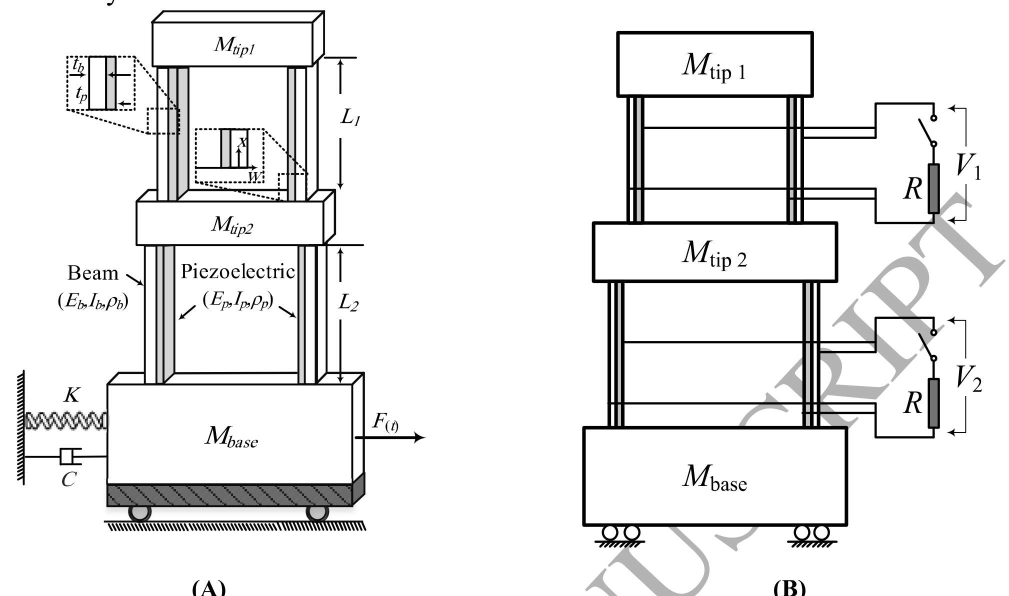

Figure1. Schematic of the clamped-guided piezoelectric beam with tip mass (A); and electrical circuit of the system (B)

Euler Bernoulli beam theory in conjunction with Lagrange's method is used to determine the differential equations of motion of the system. In this analysis, the piezoelectric materials are also modeled using Euler Bernoulli beam theory. It is assumed that only the first bending modes of the two beams, shown in Figure (1-A), are excited and therefore the resultant equations of motion are as follows (the details of this analysis are given in Appendix A).

$$m_{eq_1}\ddot{q}_{i_1} + c_{eq_1}\dot{q}_{i_1} + \left(k_{eq_1} - k_{g_1}\right)q_{i1} - \theta_1 V_1 = -m^*\ddot{q}_{i_2} \tag{1}$$

$$m_{eq_2}\ddot{q}_{i_2} + c_{eq_2}\dot{q}_{i_2} + \left(k_{eq_2} - k_{g_2}\right)q_{i2} - \theta_2 V_2 = F - m^*\ddot{q}_{i_1} \tag{2}$$

$$C_p\dot{V}_1 + V_1/R + \theta_1\dot{q}_1 = 0 \tag{3}$$

$$C_p\dot{V}_2 + V_2/R + \theta_2\dot{q}_2 = 0 \tag{4}$$

where m_{eqi} is the equivalent mass of the i^{th} mass and k_{eqi} and c_{eqi} are respectively the i^{th} equivalent stiffness and damping. Furthermore, k_{gi} and θ_{i} are the i^{th} geometric stiffness and electromechanical coupling coefficient. The coefficients of equations (1-4) are as follows:

$$m_{eq_1} = 2\int_0^{L_1}\left(\rho_b t_b w_b + \rho_p t_p w_p\right)\varphi_1^2 dx + M_{tip_1}\varphi_1^2(L_1) \tag{5}$$

$$m_{eq_2} = 2\int_0^{L_2}\left(\rho_b t_b w_b + \rho_p t_p w_p\right)\varphi_2^2 dx + \left(2\left(\rho_b t_b w_b + \rho_p t_p w_p\right)L_1 + M_{tip_1} + M_{tip_2}\right)\varphi_2^2(L_2) \tag{6}$$

$$m^* = 2\left(\rho_b t_b w_b + \rho_p t_p w_p\right)\varphi_2(L_2)\int_0^{L_1}\varphi_1 dx + M_{tip_1}\varphi_1(L_1)\varphi_2(L_2) \tag{7}$$

$$k_{eq_2} = 2\int_0^{L_2}\left(E_b I_b + E_p I_p\right)\left(\frac{d^2\varphi_2}{dx^2}\right)^2 dx \tag{8}$$

$$k_{eq1} = 2\int_0^{L_1}\left(E_b I_b + E_p I_p\right)\left(\frac{d^2\varphi_1}{dx^2}\right)^2 dx \tag{9}$$

$$k_{g_1} = N_1 \int_0^{L_1} \left(\frac{d\varphi_1}{dx} \right)^2 dx \tag{10}$$

$$k_{g_2} = N_2 \int_0^{L_2} \left(\frac{d\varphi_2}{dx} \right)^2 dx \tag{11}$$

$$c_{eq_1} = 2\zeta_1 \sqrt{k_{eq_1} m_{eq_1}} \tag{12}$$

$$c_{eq_2} = 2\zeta_2 \sqrt{k_{eq_2} m_{eq_2}} \tag{13}$$

$$\theta_1 = 2\int_{x_1}^{x_2} z\, w_p e_{31} \left(\frac{d^2\varphi_1}{dx^2} \right) dx \tag{14}$$

$$\theta_2 = 2\int_{x_1}^{x_2} z\, w_p e_{31} \left(\frac{d^2\varphi_2}{dx^2} \right) dx \tag{15}$$

$$M_{eq} = 2\left(\rho_b t_b w_b + \rho_p t_p w_p\right)\left(L_2 + L_1\right) + M_{tip_1} + M_{tip_2} + M_{base} \tag{16}$$

$$C_p = 2\int_{x_1}^{x_2} w_p e_{33} / t_p \, dx \tag{17}$$

Parameters C_{p}, V and R in the above equations are piezoelectric capacitance, output electrical voltage and the load resistance, respectively. The process of finding the equations discussed above is presented in Appendix A. Note that the geometric stiffness shows the effect of the axial loads due to the weight of tip masses on the stiffness of the beam column.

2-2- Experimental modal analysis

The theories present the system in an ideal way while uncertainty of the analytical models is one of the engineering issues. To increase modeling accuracy, the theoretical model is updated using the experimental modal data. To this end, a prototype whose properties are presented in Table (1) is tested. In this table, it should be noted that subscripts B and P refer to as beam and piezoelectric respectively.

Table1. Properties of the presented energy harvesting system device

Parameters	Values	Parameters	Values	Parameters	Values
L_{B1}(mm)	59.00	M_{tip2} (gr)	134.07	d_{31}(pC/N)	-280
L_{B2}(mm)	61.75	E_P (GPa)	62.5	e_{33} (nF/m)	6.5
L_{P1}(mm)	59.00	E_B (GPa)	170	t_B(mm)	0.15
L_{P2} (mm)	61.75	ρ_B(kg/m^3)	8500	t_P(mm)	0.11
M_{base}(gr)	311.94	ρ_P(kg/m^3)	7500	w_P(mm)	36
M_{tip1} (gr)	38.85	R (MΩ)	1	w_B(mm)	37

The experimental modal analysis is performed on the system, which is shown in part (A) of Figure (2): the system is excited by a modal hammer (Global Test AU-02) and the response is measured by accelerometers (Global Test AP2037-100). Furthermore, signal acquisition is performed using National Instruments hardware (NI 9230) with a 12.8 kHz sampling rate, which is higher than necessary to ensure any higher harmonic content is considered (frequency range of interest ≤30Hz). Note that the added mass due to the sensor (9.8gr) is considered in the analytical model. Each of the measurements obtained is the average of the responses of ten different impacts, ensuring coherence as close to the unity as possible. The frequency response of the system is shown in part (B) of Figure (2). Note that the Aij is the accelerance frequency response function, in which the input impulsive force is applied at coordinate j and the response is measured at coordinate i.

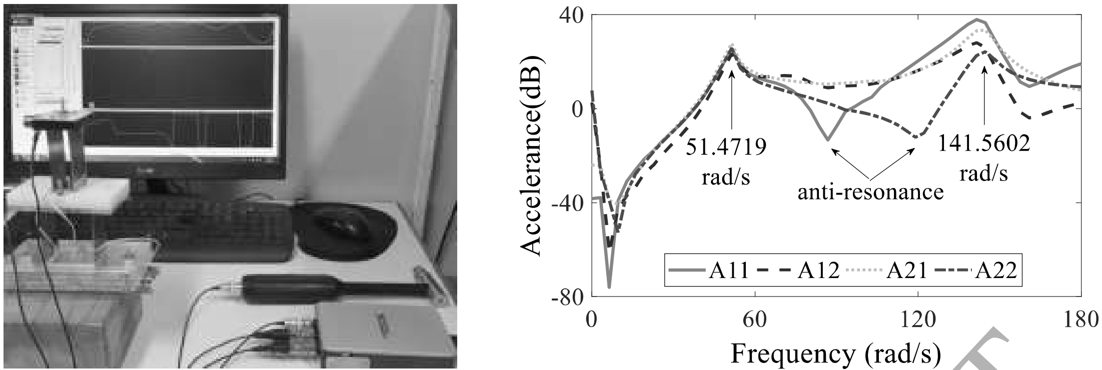

(A) (B)

Figure 2. Experimental set-up(A); and accelerance of energy harvesting system versus frequency (B)

The experiential mode shapes of vibration for the system are:

$$\Phi = \begin{bmatrix} 0.8002 & 0.9387 \\ 0.5998 & -0.3448 \end{bmatrix} \tag{18}$$

The modal mass ($\boldsymbol{\phi}^{-T}\boldsymbol{\phi}^{-1}$) and stiffness ($\boldsymbol{\phi}^{-T}\boldsymbol{\omega}_r^{2}\boldsymbol{\phi}^{-1}$) matrices can be obtained using equation (18) [35]. Here, the experimental spatial matrices will be used to improve the analytical results. To do so, the modal updating method will be used in next section.

2-3- Validating electromechanical behavior

In order to examine the accuracy of the theoretical results which are obtained using the updated analytical model, another test is performed. As shown in Figure (3), an MS-100N electromechanical shaker is attached to the base mass to provide the base excitation. The electrical power of the shaker is supplied by a LA200 power amplifier. The IEPE accelerometers (GT-AU02) are attached to the tip masses and base mass to measure acceleration. The sampling frequency of the acquisition system is considered to be 10 KHz.

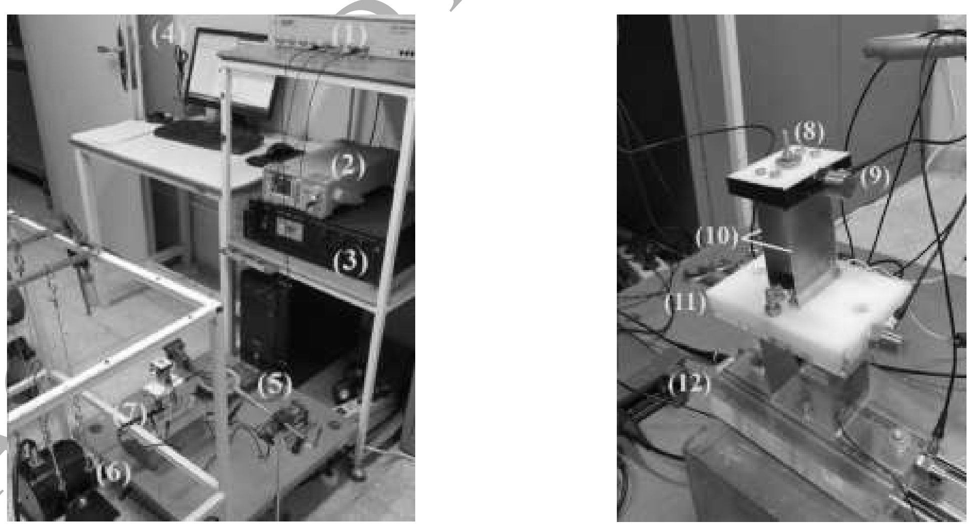

(A) (B)

1- Data acquisition system	5- Oscilloscope	9- Accelerometer
2- Signal generator	6- Shaker	10- piezoelectric beams
3- Power amplifier	7- Energy harvester	11- M_{tip2}
4- Frequency response analyzer	8-M_{tip1}	12- M_{base}

Figure3. Details of the experimental setup used in this paper (A); and the energy harvesting system (B)

The model updating method which is discussed in appendix B is used to improve theoretical result accuracy. The natural frequency and variance of mode shape (σ_{Φ}) which is introduced in appendix B are given in Table (2). In addition, for further validation the finite element analysis is presented and compared in appendix C.

Table2. Measured, initial and updated natural frequencies.

Parameter	ω_1(rad/s)	Error (%)	ω_2(rad/s)	Error (%)	σ_Φ
Experimental	51.4719	---	141.5602	---	---
Analytical	53.0479	3.0619	144.2109	1.8725	0.0452
Updated analytical (IEMM)	51.4888	0.0328	141.5793	0.0135	0.0005

The Frequency response of the system, for the first and second tip masses, with respect to the base excitation frequency is shown in parts (A) and (B) of Figure (4), respectively. This figure shows that the updated theoretical results are in good agreement with the experimental data.

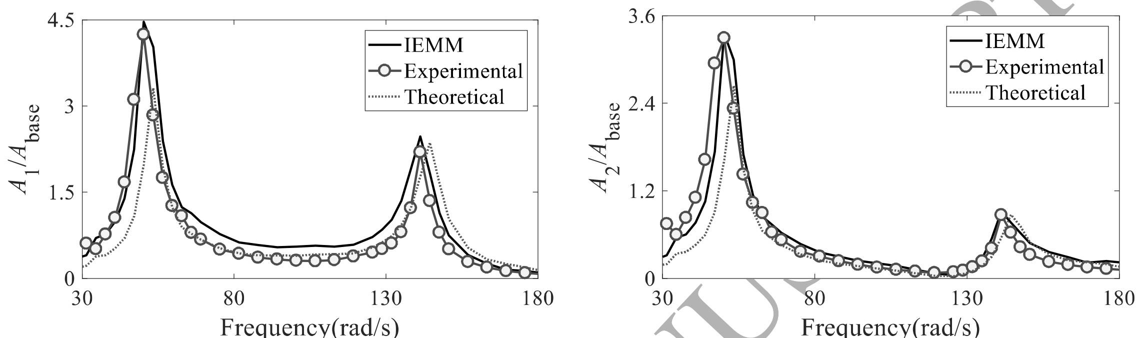

(A) **(B)**

Figure4. Experimental and theoretical frequency responses, before updating and with IEMM updating for M_{tip1} (A); M_{tip2} (B)

Furthermore, the output electrical voltage from the first and second piezoelectric layers is shown in parts (A) and (B) of Figure (5). As shown in this figure, the theoretical results accurately follow the experimental results. Therefore, it can be concluded that the updated equations of motion accurately describe the electromechanical behavior of the energy harvester. It should be noted that the damping ratios ζ_1 and ζ_2 should be obtained experimentally. To this end, the damping ratios in the updated theoretical model are changed to find frequency responses with peaks near to the peaks of the experimental frequency response. Using this procedure, the damping ratios are obtained and they are equal to ζ_1=0.044 and ζ_2=0.023.

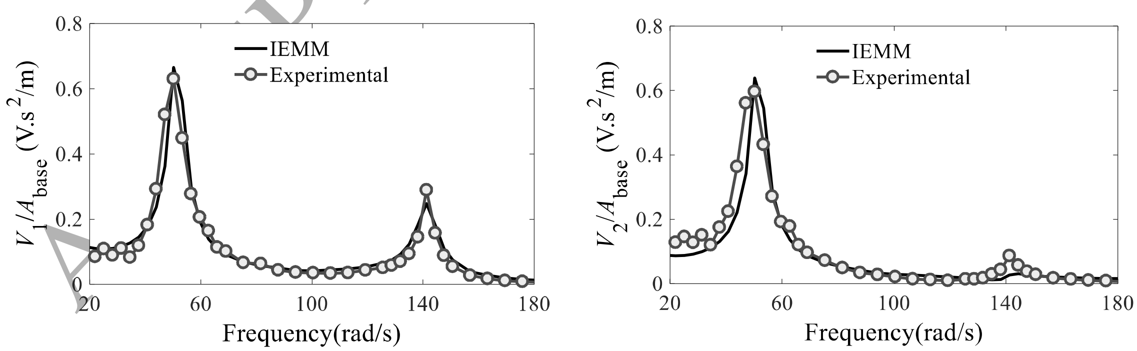

(A) **(B)**

Figure 5. Ooutput voltage of M_{tip1} (C); M_{tip2} (D) of the piezoelectric energy harvesting system

3- Novel oceanic application

3-1- breaking wave force

When ocean waves directly break on a vertical-faced coastal structure, an impulsive pressure is produced which can be extremely high in magnitude and short in duration in comparison with non-breaking waves. In the present study, the breaking waves are the desired input force to the energy harvester system. This is mainly because the breaking waves has high energy density compared to other ocean waves. Generally, at the breaking point simple linear physical models which describe wave dynamics become invalid. Thus, experimental results are the best way to find a good estimation of their dynamic behavior. Part (A) of Figure (6) illustrates breaking wave force, which is obtained by experiment [36]. Other parameters of the experiment are presented in Table (3). The Power Spectral Density (PSD) of the breaking wave force signal is shown in part (B) of Figure (6). As shown in this figure, the wave can effectively excite the system in the frequency range of 1~20 rad/s (zone I). Furthermore, it can be concluded that between 20 and 100 rad/s, the excitation level is good (zone II) and in 100~250 rad/s the excitation level is acceptable (zone III). Note that the presented power spectral density in part (B) of Figure (6) belongs to the impulsive load of the ocean waves and the dynamic properties of the energy harvester should be selected based on a frequency range of 0 to 250 rad/s. In other words, the presented energy harvesting system can effectively work in finite frequencies in the presented broad frequency range (natural frequencies of energy harvester).

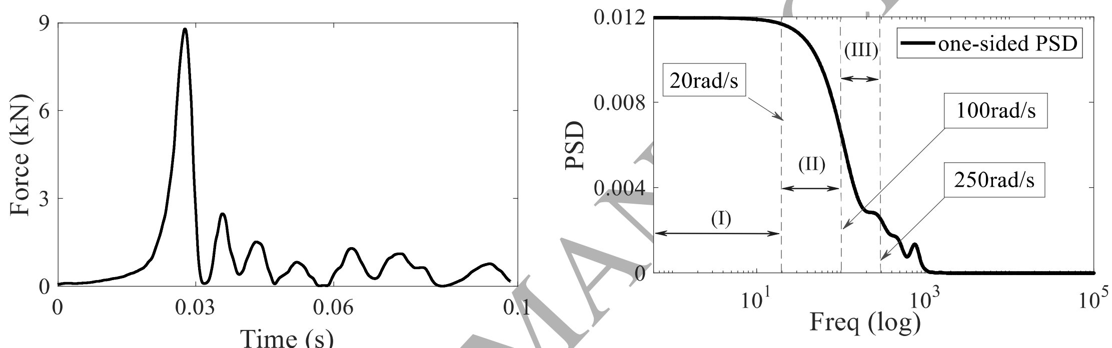

(A) **(B)**

Figure6. The amplitude of force (A) [36]; and properties of experimental breaking wave on a vertical face

Figure (6-A) shows that the breaking wave could be considered an impulsive force with the properties presented in Table (3). One may conclude that the experimental condition is shallow water, which is near to realistic condition.

Table3. Properties of the breaking waves

Parameter	Amplitude
Wave period	2 sec
Deep water wave height	H_0=0.277 m
Deep-water wave steepness	H_0/L_0=0.044

2-2- The wave breaker and energy harvesting device

In order to reduce wave damage effects on in-shore structures, wave breakers are constructed. For example, the total length of breakwaters in Japan is more than 800 km, which can give the reader a feeling of the importance of these structures [37]. Rubble mound breakwaters are a popular type of breakwaters which can damp ocean wave energy in a simple and low cost way [38, 39]. In this study, the rubble mound breakwater, which plays a multifunctional role as both wave breaker and energy collector, is shown in Figure (7).

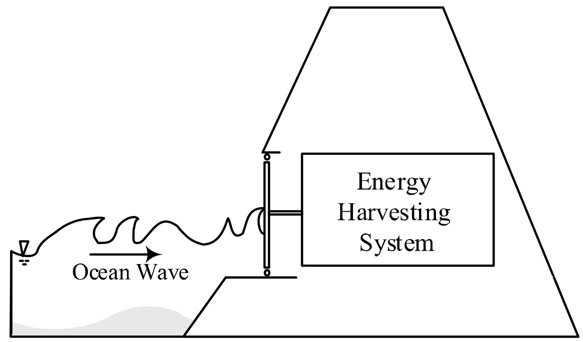

Figure7. Sketch of the energy harvester mounted in breakwater

Figure 7 shows the main idea of this paper. As can be seen in this figure, a vibration-based energy harvesting system can be designed to extract energy from the ocean wave that are breaking on a vertical wall. In this paper, for the first time to the authors' knowledge, we demonstrate how a 2 degree of freedom vibration-based piezoelectric harvesting system may be used to extract energy from the ocean wave. In other words, contribution of this paper concerns the proof of concept and the detailed design of such a system will be investigated in future studies.

4- Analysis of the wave breaker energy-harvesting device

Increasing strain in the piezoelectric beams leads to an increase in the generated voltage from the presented system. Therefore, finding a way to increase strain in the piezoelectric beam columns results in improving the power generation in the discussed system. To do so, a combination of the following energy harvesting systems can be used. Four configurations are presented in parts (A) to (D) of Figure (8).

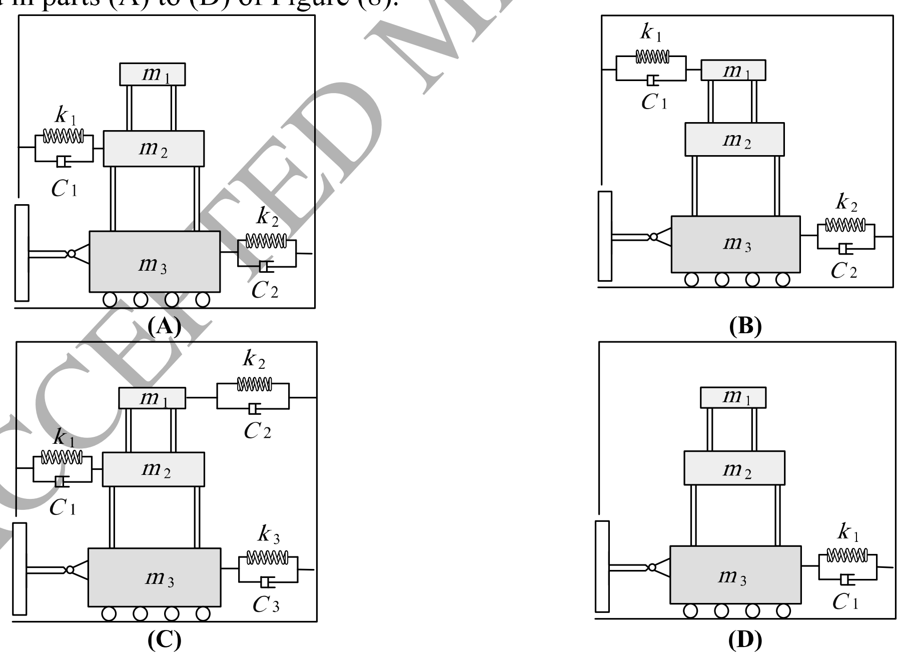

Figure8. The first (A); second (B); third (C) and fourth (D) configurations for the energy harvesting system

Assuming the first frequency resonance of the system is equal to the frequency of ocean waves, the frequency response function of the system is shown in Figure (9). In this figure H_{ij} is the displacement at coordinate *i* due to a single force at coordinate *j* (receptance). Note that all stiffness in the first configuration should be equal to 213.7942 N/m in order to have a system with a fundamental frequency near to the ocean wave frequency. For the second, third and fourth configurations, assumed stiffness values should be equal to 196.7496 N/m, 126.4096 N/m and 605.641 N/m respectively. The calculated spring stiffness and the first three natural frequencies of the energy harvesting system are shown in Table (4). All the first three natural frequencies of the presented system which can be observed in Figure (9) occurred in distinguished zones in the PSD diagram (Figure 6-B).

Table4. Stiffness of springs, used in the energy harvesting systems and their corresponding natural frequencies

Configuration → Parameters ↓	First	Second	Third	Fourth
k (N/m)	213.7942	196.7496	126.4096	605.641
ω_1 (rad/s)	3.1416	3.1416	3.1416	3.1416
ω_2 (rad/s)	85.5147	88.0460	87.0697	88.4631
ω_3 (rad/s)	143.6111	148.4744	146.7602	142.7276

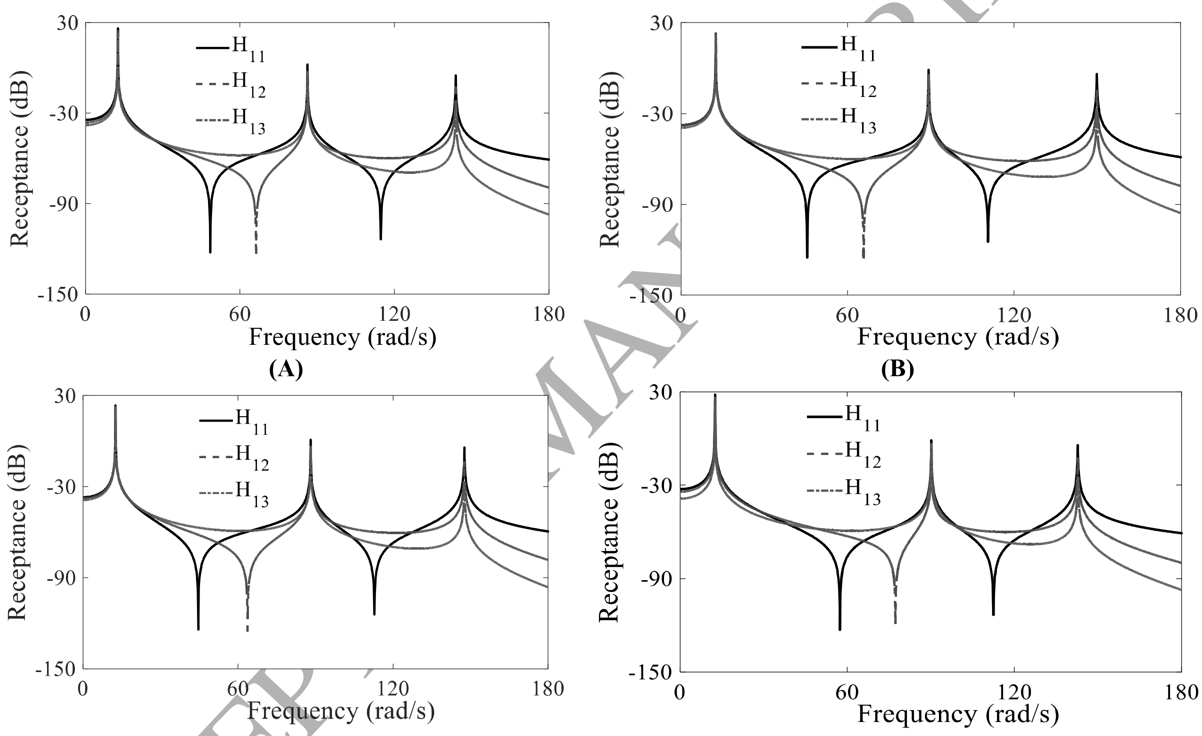

Figure9. Frequency response for the first (A); second (B); third (C); and fourth (D) configuration

The piezoelectric beam-column energy harvesters considered are connected in series and the root mean square output voltage ($V_{tot.rms}$) of different configurations in the first natural frequency of the system is shown in Figure (10). Note that the excitation force in this figure is equal to the ocean wave force, shown in part (A) of Figure (1).

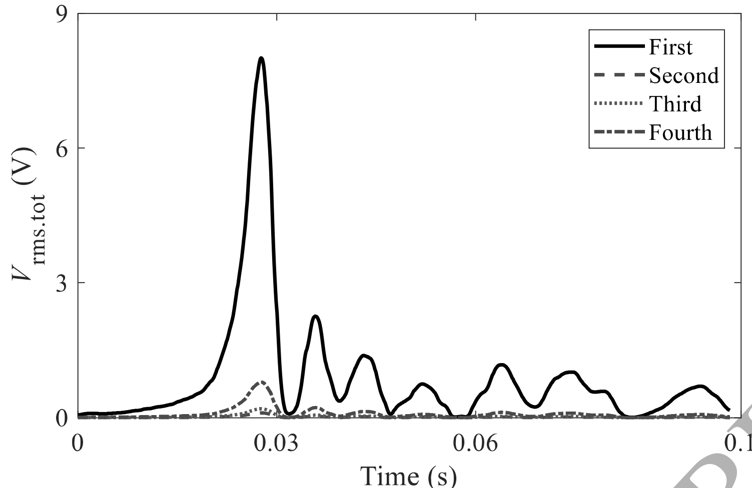

Figure10. Frequency response of RMS voltage for the different configurations under breaking wave (R=1MΩ)

As shown in Figure (10), the RMS output voltage from the first configuration is larger than other configurations because spring k_1 provides a constraint which leads to an increase in the strain rate in the first beam-column and produces more voltage than other configurations. Therefore, the first configuration is the best option for harvesting energy from ocean waves. The energy harvesting system with the first configuration can produce 6.054 V. Figure (10) shows that the first and then the fourth configurations can harvest the largest electrical voltage. The reason for this behavior lies in the fact that the relative motions of the masses in these configurations are greater than in other configurations. The relative motion of masses in each of the four configurations is shown in Figure (11).

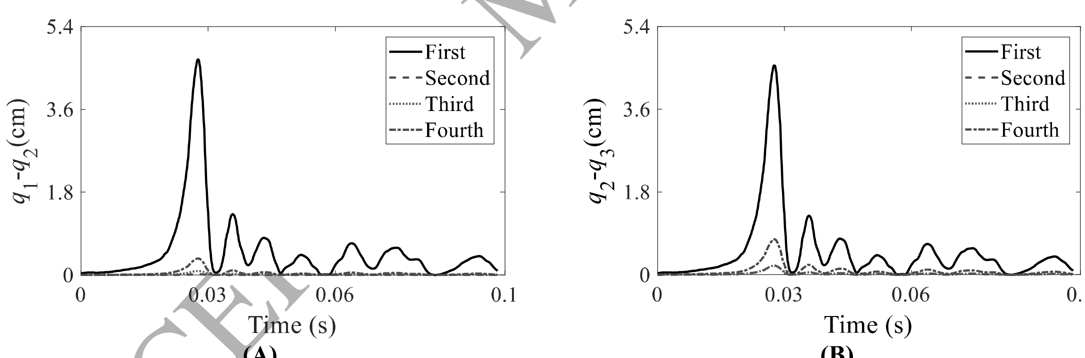

Figure11. The relative motion between m_1 and m_2 (A) and between m_2 and m_3 (B) for first, second, third and fourth configurations

To ensure a reliable structure, issues other than electrical voltage should be considered. It is clear that increasing the relative displacement of masses which leads to an increase in the strain rate and consequently in output voltage, may result in mechanical damage to the system. Perfection Rate (PR) is introduced in this paper to determine the best compromise between the positive effect of increasing voltage and negative effect of increasing the relative motion in a parameter. The PR parameter is defined as follows:

$$PR = 100\left\{WF \times \frac{V}{V_{\max}} + \left(1 - WF\right) \times \left(1 - \frac{RM}{RM_{\max}}\right)\right\} \tag{19}$$

where *RM* is relative motion and weight factor (*WF*) is a criterion, to show the importance of relative motion and output voltage in decision makings. Note that the $RM_{\max}$ is the relative motion between the first and second masses (q_1-q_2) at the first natural frequency. The *PR* for three different weight factors is shown in Figure (12).

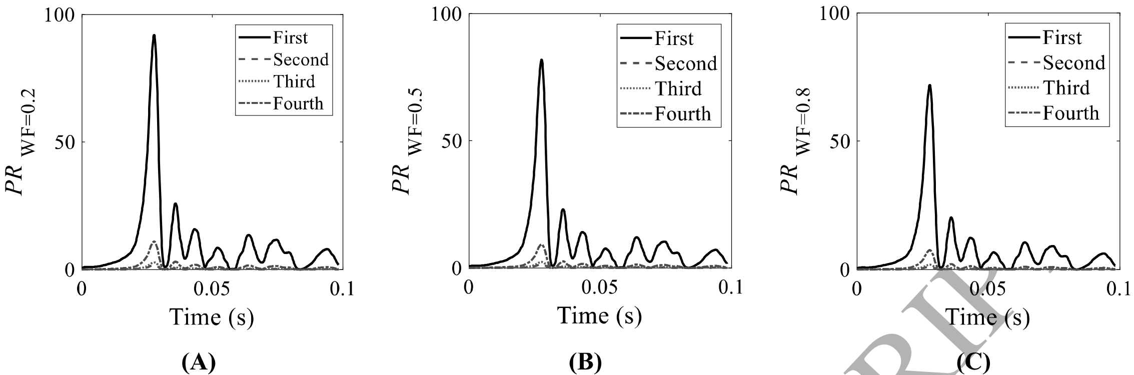

Figure12. PR for *WF*=0.2 (A), *WF*=0.5 (B) and *WF*=0.8 (C) for first, second, third and fourth configurations

Wave breakers often operate in difficult environments and the use of an external power supply for the remote sensors of these structures is not affordable. Hence, techniques to integrate an energy harvesting system into these structures deemed necessary. In case of ocean wave breaker, large amplitude of force and low frequency, leads to design given structures in this study. As shown in Figure (12), for weight factors between 0.2 and 0.8, the first and forth configurations are the best designs for the energy harvesting systems presented. Furthermore, the smallest *PR* belongs to the second configuration. These piezoelectric structures are inherently vibration isolator and energy harvesters, which are likely to be the best. Future research will investigate the possibility of using electromagnetic devices. It is worth noting that the proposed system can be re-designed in the form of mechanical metamaterial. In this category, wave filtering and energy harvesting can be achieved simultaneously [40-42]. Although it cannot be used in this study due to placement constraint, future research can be concentrated on the possibility of using this system in the metamaterial category.

5- Conclusion

The demand for energy is one of the most crucial issues for the future of human beings. While the ocean which generates high power covers most of Earth's surface, its energy is easily wasting around us. Because of the high energy density of violent breaking waves, considering a vertical-face in rubble mount breakwaters could be an intelligent suggestion. In terms of energy harvesting, a conceptual model including a beam-column piezoelectric energy harvester which can work in a binary frequency domain is introduced in order to reduce the size of energy harvesters. A mathematical model of the energy harvester which is derived to describe the application of the system is updated by the experimental results and, after validation, is used to study energy harvesting from ocean waves. In order to maximize the harvested energy, the behavior of four possible configurations was investigated. To study both the lifespan of the structure and the harvested energy, the so-called Perfection Rate is introduced. Ultimately, it was concluded that a special configuration (the first configuration in this study) would be the better choice for energy harvesting. It has been shown that when the WF=0.5, the Perfection Rate for this configuration can be higher than other configurations by more than 46%.

Appendix A

According to the Euler-Bernoulli beam theory, the equation for the potential energy of the presented system is as follows:

$$\pi = \int_0^{L_1} \left(EI_b + EI_p\right)\left(\frac{\partial^2 w_1}{\partial x^2}\right)^2 dx + \int_0^{L_2} \left(EI_b + EI_p\right)\left(\frac{\partial^2 w_2}{\partial x^2}\right)^2 dx - \int_0^{L_1} z w_p V e_{31}\left(\frac{\partial^2 w_1}{\partial x^2}\right) dx$$
$$- \int_0^{L_2} z w_p V e_{31}\left(\frac{\partial^2 w_2}{\partial x^2}\right) dx + \frac{1}{2} K Z^2 \tag{A.1}$$

where $w(x,t)$ and V are the transverse displacement of the beam and electrical voltage. Furthermore, e_{31} is the effective piezoelectric stress constant. The kinetic energy for the system can be written as follows:

$$T = \int_0^{L_1} \left(\rho_b t_b w_b + \rho_p t_p w_p\right)\left(\frac{\partial w_1}{\partial t} + \frac{\partial w_2}{\partial t}\Big|_{x=L_2} + \dot{Z}\right)^2 dx + \frac{1}{2} M_{tip2}\left(\dot{Z} + \frac{\partial w_2}{\partial t}\Big|_{x=L_2}\right)^2$$
$$\int_0^{L_1} \left(\rho_b t_b w_b + \rho_p t_p w_p\right)\left(\frac{\partial w_2}{\partial t} + \dot{Z}\right)^2 dx + \frac{1}{2} M_{base}\dot{Z}^2 + \tag{A.2}$$
$$\frac{1}{2} M_{tip1}\left(\dot{Z} + \frac{\partial w_1}{\partial t}\Big|_{x=L_1} + \frac{\partial w_2}{\partial t}\Big|_{x=L_2}\right)^2$$

where w_b and w_p are the beam and piezoelectric width, respectively. The internal electrical energy in the presented system can be given by:

$$W_{ie} = -\int_{x_1}^{x_2} w_p V \left\{ e_{31}\left(-z\frac{\partial^2 w}{\partial x^2}\right) - e_{33}\frac{V}{t_p} \right\} dx \tag{A.3}$$

where e_{33} is the permittivity component at constant strain and the piezoelectric layer width. The non-conservative virtual work of the system is written as follows:

$$\delta W_e = F\,\delta Z + N\int_0^L \frac{\partial w}{\partial x}\delta\left(\frac{\partial w}{\partial x}\right) dx - Q\,\delta V - f_d\,\delta q - C\dot{Z}_i\,\delta Z \tag{A.4}$$

where N is the axial load, and in this study is equal to M_{tip}g, and F is the external load. Using the separation of variable method, displacement of the beam can be given as follows:

$$w_j(x,t) = \sum_{i=1}^{n} \varphi_{ij}(x) q_{ij}(t) \tag{A.5}$$

where $\varphi(x)$ and $q(t)$ indicate mode shape and time response. The electro-mechanical Lagrange equations can be expressed as [43]:

$$\frac{d}{dt}\left(\frac{\partial T}{\partial \dot{q}_i}\right) - \frac{\partial T}{\partial q_i} + \frac{\partial \pi}{\partial q_i} - \frac{\partial W_{ie}}{\partial q_i} = N\, q_i \int_0^L \left(\frac{d\varphi}{dx}\right)^2 dx - f_d \tag{A.6}$$

$$\frac{d}{dt}\left(\frac{\partial T}{\partial \dot{Z}}\right) - \frac{\partial T}{\partial Z} + \frac{\partial \pi}{\partial Z} - \frac{\partial W_{ie}}{\partial Z} = F - C\dot{Z} \tag{A.7}$$

$$\frac{d}{dt}\left(\frac{\partial T}{\partial \dot{V}}\right) - \frac{\partial T}{\partial V} + \frac{\partial \pi}{\partial V} - \frac{\partial W_{ie}}{\partial V} = Q \tag{A.8}$$

where Q is the electric charge output and f_d is the damping force, which can be obtained using the Rayleigh damping theory. Substituting Eq (A.4) into Eq's (A.1-A.3) and according to the Lagrange equations, the following relations are obtained for constants of equations (1-4):

$$m_{eq_1} = 2\int_0^{L_1} \left(\rho_b t_b w_b + \rho_p t_p w_p\right)\varphi_1^2 dx + M_{tip_1}\varphi_1^2(L_1) \tag{A.9}$$

$$m_{eq_2} = 2\int_0^{L_2} \left(\rho_b t_b w_b + \rho_p t_p w_p\right)\varphi_2^2 dx + \left(2\left(\rho_b t_b w_b + \rho_p t_p w_p\right)L_1 + M_{tip_1} + M_{tip_2}\right)\varphi_2^2(L_2) \tag{A.10}$$

$$m^* = 2\left(\rho_b t_b w_b + \rho_p t_p w_p\right)\varphi_2(L_2)\int_0^{L_1} \varphi_1 dx + M_{tip_1}\varphi_1(L_1)\varphi_2(L_2) \tag{A.11}$$

$$k_{eq_2} = 2\int_0^{L_2} \left(E_b I_b + E_p I_p\right)\left(\frac{d^2\varphi_2}{dx^2}\right)^2 dx \tag{A.12}$$

$$k_{eq1} = 2\int_0^{L_1} \left(E_b I_b + E_p I_p\right)\left(\frac{d^2\varphi_1}{dx^2}\right)^2 dx \tag{A.13}$$

$$k_{g_1} = N_1\int_0^{L_1} \left(\frac{d\varphi_1}{dx}\right)^2 dx \tag{A.14}$$

$$k_{g_2} = N_2\int_0^{L_2} \left(\frac{d\varphi_2}{dx}\right)^2 dx \tag{A.15}$$

$$c_{eq_1} = 2\zeta_1\sqrt{k_{eq_1} m_{eq_1}} \tag{A.16}$$

$$c_{eq_2} = 2\zeta_2\sqrt{k_{eq_2} m_{eq_2}} \tag{A.17}$$

$$\theta_1 = 2\int_{x_1}^{x_2} z\, w_p e_{31}\left(\frac{d^2\varphi_1}{dx^2}\right)dx \tag{A.18}$$

$$\theta_2 = 2\int_{x_1}^{x_2} z\, w_p e_{31}\left(\frac{d^2\varphi_2}{dx^2}\right)dx \tag{A.19}$$

$$M_{eq} = 2\left(\rho_b t_b w_b + \rho_p t_p w_p\right)\left(L_2 + L_1\right) + M_{tip_1} + M_{tip_2} + M_{base} \tag{A.20}$$

$$C_p = 2\int_{x_1}^{x_2} w_p e_{33}/t_p\, dx \tag{A.21}$$

In the above equations, ζ is the damping ratio. According to the Euler-Bernoulli theory, the mode shape of the vibration of the beam with length L can be written as follows:

$$\varphi_i(x) = C_i\left\{\cos\left(\lambda_i x/L\right) - \cosh\left(\lambda_i x/L\right) + \sigma_i\left(\sin\left(\lambda_i x/L\right) - \sinh\left(\lambda_i x/L\right)\right)\right\} \tag{A.22}$$

where λ_i is the eigenvalue of the i^{th} vibration mode, that can be obtained using the characteristic equation, which is derived according to the eigenfunction and the boundary conditions. The characteristic equation can be obtained as follows:

$$1 - \cos\left(\lambda_i\right)\cosh\left(\lambda_i\right) - \frac{\rho A L}{\lambda_i M_{tip}}\left(\cos\left(\lambda_i\right)\sinh\left(\lambda_i\right) + \cosh\left(\lambda_i\right)\sin\left(\lambda_i\right)\right) = 0 \tag{A.23}$$

Note that ω_i is the un-damped natural frequency of the i^{th} vibration mode ($\omega^2 = EI\lambda^4/(\rho AL)$) and σ_i is a coefficient, which can be calculated using the following equation:

$$\sigma_i = \frac{\left(\sin\left(\lambda_i\right) - \sinh\left(\lambda_i\right)\right) + \frac{M_{tip}\lambda_i}{\rho A L}\left(\cos\left(\lambda_i\right) - \cosh\left(\lambda_i\right)\right)}{\left(\cos\left(\lambda_i\right) + \cosh\left(\lambda_i\right)\right) - \frac{M_{tip}\lambda_i}{\rho A L}\left(\sin\left(\lambda_i\right) - \sinh\left(\lambda_i\right)\right)} \tag{A.24}$$

Appendix B

The Error Matrix Method (EMM) is the updating method used in this paper [35]. This method is a direct procedure with assured convergence, which adjusts analytical mass and stiffness matrices with the following error stiffness and mass matrices [35, 44]:

$$\Delta K = [K_A]\left\{[\phi_A][\omega_{Ar}^2]^{-1}[\phi_A]^T - [\phi_X][\omega_{Xr}^2]^{-1}[\phi_X]^T\right\}[K_A] \tag{B.1}$$

$$\Delta M = [M_A]\left\{[\phi_A][\phi_A]^T - [\phi_X][\phi_X]^T\right\}[M_A] \tag{B.2}$$

where A and X refer to analytical and experimental results. In this study, the EMM procedure is modified using the mode shape variance, which is defined as follows:

$$\sigma_\Phi = \sqrt{\sum_{i,j=1}^{n}\left(\mathrm{MAC}_{ij}-\delta_{ij}\right)^2}\Big/2n \tag{B.3}$$

where δ is the Kronecker delta. The procedure of the presented updating method, which is simply named as Iterative Error Matrix Method (IEMM), is shown in part (A) of Figure (B.1.). During the updating procedure, it is considered that the sum of the diagonal elements of the updated mass matrix is constant and equal to the total mass of the studied vibratory system. Furthermore, natural frequency error and the overall mode shape error indicator in each iteration number is depicted in part (B) of Figure (B.1.). The MAC charts for the results before and after updating are shown in part (C) and part (D) of Figure (B.1.) respectively.

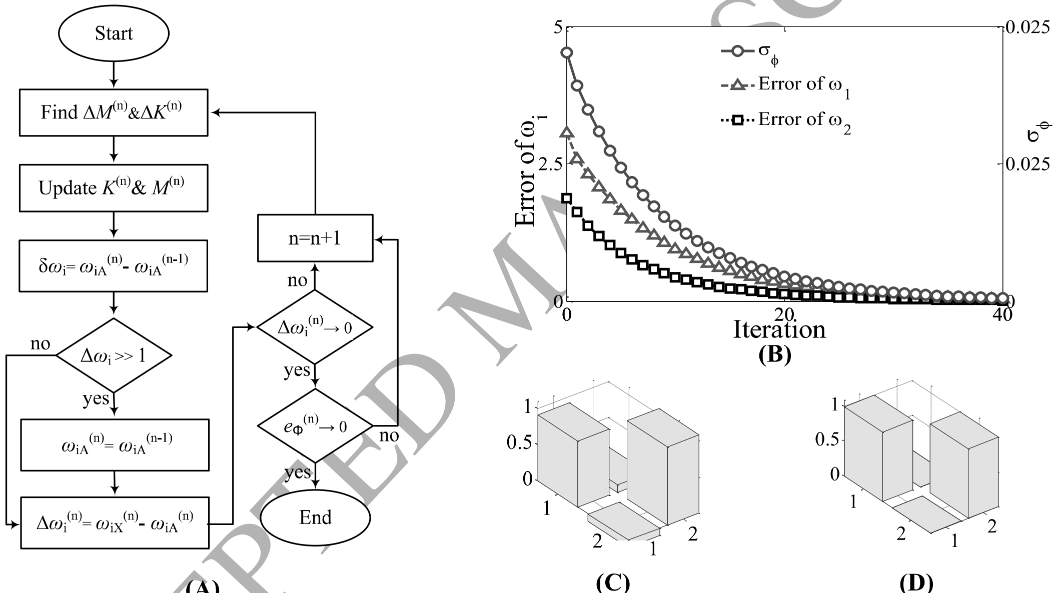

Figure B.1. Flowchart of the IEMM (A); variation of natural frequency error and overall mode shape error indicator with varying iteration number (B); MAC chart for n=0 (C); and MAC chart for n=40 (D)

According to part (C) of Figure (B.1.), it can be concluded that by increasing the iteration number, the first and second frequency errors decrease. Natural frequency errors and the mode shape variance, decrease by increasing the iteration number.

Appendix C

A finite Element based academic software is used to model the proposed systems. f The first and second mode shapes and their corresponding natural frequencies are shown in parts (A) and (B) of Figure (C.1.) respectively.

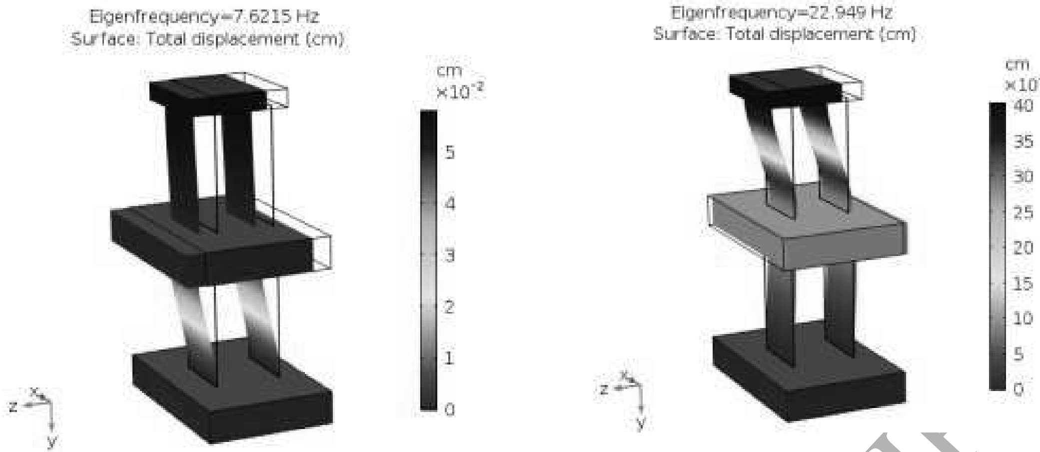

(A) **(B)**

Figure C.1. Finite element modal behavior of the proposed system in the first(A); and second (B) natural frequency

As it can be seen in Figure C.1, in the first two mode shapes of the proposed system the clamped-guided systems oscillate with their first mode shape. Therefore, using a single mode for modelling of the system might be a reasonable assumption. Furthermore, as shown in table C.1, the presented result for the first and second natural frequencies follows experimental and analytical behaviors of the system.

Table C.1. Modeled, measured, initial and updated natural frequencies

Parameter	$\boldsymbol{\omega_1}$ (rad/s)	Error (%)	$\boldsymbol{\omega_2}$ (rad/s)	Error (%)
Experimental	51.4719	---	141.5602	---
Analytical	53.0479	3.0619	144.2109	1.8725
Simulation	47.8873	6.9642	144.1928	1.8597
Updated analytical	51.4888	0.0328	141.5793	0.0135

Acknowledgment

Hamed Haddad Khodaparast acknowledges the support provided by the EPSRC through grant number EP/P01271X/1.

Reference

[1] A. Ressurreição, J. Gibbons, T. P. Dentinho, M. Kaiser, R. S. Santos, and G. Edwards-Jones, "Economic valuation of species loss in the open sea," *Ecological Economics,* vol. 70, pp. 729-739, 2011.

[2] F. d. O. Antonio, "Wave energy utilization: A review of the technologies," *Renewable and sustainable energy reviews,* vol. 14, pp. 899-918, 2010.

[3] I. López, J. Andreu, S. Ceballos, I. M. de Alegría, and I. Kortabarria, "Review of wave energy technologies and the necessary power-equipment," *Renewable and Sustainable Energy Reviews,* vol. 27, pp. 413-434, 2013.

[4] A. Uihlein and D. Magagna, "Wave and tidal current energy–A review of the current state of research beyond technology," *Renewable and Sustainable Energy Reviews,* vol. 58, pp. 1070-1081, 2016.

[5] A. de Andres, A. MacGillivray, O. Roberts, R. Guanche, and H. Jeffrey, "Beyond LCOE: A study of ocean energy technology development and deployment attractiveness," *Sustainable Energy Technologies and Assessments,* vol. 19, pp. 1-16, 2017.

[6] N. Khan, A. Kalair, N. Abas, and A. Haider, "Review of ocean tidal, wave and thermal energy technologies," *Renewable and Sustainable Energy Reviews,* vol. 72, pp. 590-604, 2017.

[7] M. Melikoglu, "Current status and future of ocean energy sources: A global review," *Ocean Engineering,* vol. 148, pp. 563-573, 2018.

[8] R. C. Lisboa, P. R. Teixeira, and C. J. Fortes, "Numerical evaluation of wave energy potential in the south of Brazil," *Energy,* vol. 121, pp. 176-184, 2017.

[9] A. Ulazia, M. Penalba, G. Ibarra-Berastegui, J. Ringwood, and J. Saénz, "Wave energy trends over the Bay of Biscay and the consequences for wave energy converters," *Energy,* vol. 141, pp. 624-634, 2017.

[10] J. Xie and L. Zuo, "Dynamics and control of ocean wave energy converters," *International Journal of Dynamics and Control,* vol. 1, pp. 262-276, 2013.

[11] C. Liang, J. Ai, and L. Zuo, "Design, fabrication, simulation and testing of an ocean wave energy converter with mechanical motion rectifier," *Ocean Engineering,* vol. 136, pp. 190-200, 2017.

[12] J. Ai, H. Lee, C. Liang, and L. Zuo, "Ocean wave energy harvester with a novel power takeoff mechanism," in *ASME 2014 International Design Engineering Technical Conferences and Computers and Information in Engineering Conference*, 2014, pp. V008T11A086-V008T11A086.

[13] J. Scruggs and P. Jacob, "Harvesting ocean wave energy," *Science,* vol. 323, pp. 1176-1178, 2009.

[14] C. Iuppa, L. Cavallaro, E. Foti, and D. Vicinanza, "Potential wave energy production by different wave energy converters around Sicily," *Journal of Renewable and Sustainable Energy,* vol. 7, p. 061701, 2015.

[15] M. Buccino, D. Stagonas, and D. Vicinanza, "Development of a composite sea wall wave energy converter system," *Renewable Energy,* vol. 81, pp. 509-522, 2015.

[16] G. Malara, A. Romolo, V. Fiamma, and F. Arena, "On the modelling of water column oscillations in U-OWC energy harvesters," *Renewable Energy,* vol. 101, pp. 964-972, 2017.

[17] D. Ning, R. Wang, and C. Zhang, "Numerical Simulation of a Dual-Chamber Oscillating Water Column Wave Energy Converter," *Sustainability,* vol. 9, p. 1599, 2017.

[18] M. Buccino, D. Banfi, D. Vicinanza, M. Calabrese, G. D. Giudice, and A. Carravetta, "Non breaking wave forces at the front face of seawave slotcone generators," *Energies,* vol. 5, pp. 4779-4803, 2012.

[19] D. Vicinanza, J. H. Nørgaard, P. Contestabile, and T. L. Andersen, "Wave loadings acting on overtopping breakwater for energy conversion," *Journal of Coastal Research,* vol. 65, pp. 1669-1674, 2013.

[20] D. Vicinanza, P. Contestabile, J. Q. H. Nørgaard, and T. L. Andersen, "Innovative rubble mound breakwaters for overtopping wave energy conversion," *Coastal Engineering,* vol. 88, pp. 154-170, 2014.

[21] P. Contestabile, V. Ferrante, E. Di Lauro, and D. Vicinanza, "Prototype overtopping breakwater for wave energy conversion at port of Naples," in *The 26th International Ocean and Polar Engineering Conference*, 2016.

[22] P. Contestabile, C. Iuppa, E. Di Lauro, L. Cavallaro, T. L. Andersen, and D. Vicinanza, "Wave loadings acting on innovative rubble mound breakwater for overtopping wave energy conversion," *Coastal Engineering,* vol. 122, pp. 60-74, 2017.

[23] F. He, Z. Huang, and A. W.-K. Law, "An experimental study of a floating breakwater with asymmetric pneumatic chambers for wave energy extraction," *Applied energy,* vol. 106, pp. 222-231, 2013.

[24] W. Peng, K.-H. Lee, N. Mizutani, and X. Huang, "Experimental and numerical study on hydrodynamic performance of a wave energy converter using wave-induced motion of floating body," *Journal of Renewable and Sustainable Energy,* vol. 7, p. 053106, 2015.

[25] W. Peng, X. Huang, Y. Fan, J. Zhang, and X. Ren, "Numerical analysis and performance optimization of a submerged wave energy converting device based on the floating breakwater," *Journal of Renewable and Sustainable Energy,* vol. 9, p. 044503, 2017.

[26] H.-C. Zhang, D.-L. Xu, C.-R. Liu, and Y.-S. Wu, "A Floating Platform with Embedded Wave energy harvesting arrays in regular and irregular seas," *Energies,* vol. 10, p. 1348, 2017.

[27] P. Boccotti, "Design of breakwater for conversion of wave energy into electrical energy," *Ocean engineering,* vol. 51, pp. 106-118, 2012.

[28] N. Viet, X. Xie, K. Liew, N. Banthia, and Q. Wang, "Energy harvesting from ocean waves by a floating energy harvester," *Energy,* vol. 112, pp. 1219-1226, 2016.

[29] A. Afsharfard and A. Farshidianfar, "Application of single unit impact dampers to harvest energy and suppress vibrations," *Journal of Intelligent Material Systems and Structures,* vol. 25, pp. 1850-1860, 2014.

[30] A. Afsharfard, "Application of nonlinear magnetic vibro-impact vibration suppressor and energy harvester," *Mechanical Systems and Signal Processing,* vol. 98, pp. 371-381, 2018.

[31] M. Abbasi and A. Afsharfard, "Modeling and experimental study of a hand tremor suppression system," *Mechanism and Machine Theory,* vol. 126, pp. 189-200, 2018.

[32] R. Harne and K. Wang, "A review of the recent research on vibration energy harvesting via bistable systems," *Smart materials and structures,* vol. 22, p. 023001, 2013.

[33] R. Davis and M. McDowell, "Combined Euler column vibration isolation and energy harvesting," *Smart Materials and Structures,* vol. 26, p. 055001, 2017.

[34] S. F. Nabavi, A. Farshidianfar, and A. Afsharfard, "Novel piezoelectric-based ocean wave energy harvesting from offshore buoys," *Applied Ocean Research,* vol. 76, pp. 174-183, 2018.

[35] D. J. Ewins, *Modal testing: theory and practice* vol. 15: Research studies press Letchworth, 1984.
[36] M. S. Kirkgöz, "An experimental investigation of a vertical wall response to breaking wave impact," *Ocean Engineering,* vol. 17, pp. 379-391, 1990.
[37] M. Esteban, H. Takagi, and T. Shibayama, *Handbook of coastal disaster mitigation for engineers and planners*: Butterworth-Heinemann, 2015.
[38] M. O. Muttray and H. Oumeraci, "Theoretical and experimental study on wave damping inside a rubble mound breakwater," *Coastal engineering,* vol. 52, pp. 709-725, 2005.
[39] S. K. Park, A. A. Dodaran, C. S. Han, and M. E. M. Shahmirzadi, "Effects of vertical wall and tetrapod weights on wave overtopping in rubble mound breakwaters under irregular wave conditions," *International Journal of Naval Architecture and Ocean Engineering,* vol. 6, pp. 947-964, 2014.
[40] S. Gonella, A. C. To, and W. K. Liu, "Interplay between phononic bandgaps and piezoelectric microstructures for energy harvesting," *Journal of the Mechanics and Physics of Solids,* vol. 57, pp. 621-633, 2009.
[41] Y. Li, E. Baker, T. Reissman, C. Sun, and W. K. Liu, "Design of mechanical metamaterials for simultaneous vibration isolation and energy harvesting," *Applied Physics Letters,* vol. 111, p. 251903, 2017.
[42] W. Jiao and S. Gonella, "Intermodal and Subwavelength Energy Trapping in Nonlinear Metamaterial Waveguides," *Physical Review Applied,* vol. 10, p. 024006, 2018.
[43] A. Erturk and D. J. Inman, *Piezoelectric energy harvesting*: John Wiley & Sons, 2011.
[44] S. Z. Rad, "Methods for updating numerical models in structural dynamics," Department of Mechanical Engineering, Imperial College, 1997.

Graphical abstrect